

PAPER • OPEN ACCESS

# Signatures of a sampling quantum advantage in driven quantum many-body systems

To cite this article: Jirawat Tangpanitanon *et al* 2023 *Quantum Sci. Technol.* **8** 025019

View the [article online](#) for updates and enhancements.

You may also like

- [Analytical framework for quantum alternating operator ansätze](#)  
Stuart Hadfield, Tad Hogg and Eleanor G Rieffel
- [Simulating quantum materials with digital quantum computers](#)  
Lindsay Bassman, Miroslav Urbanek, Mekena Metcalf et al.
- [Quantum logic and entanglement by neutral Rydberg atoms: methods and fidelity](#)  
Xiao-Feng Shi

# Quantum Science and Technology



## PAPER

# Signatures of a sampling quantum advantage in driven quantum many-body systems

### OPEN ACCESS

RECEIVED  
14 August 2022

REVISED  
12 January 2023


ACCEPTED FOR PUBLICATION  
20 February 2023

PUBLISHED  
13 March 2023

Original Content from this work may be used under the terms of the [Creative Commons Attribution 4.0 licence](https://creativecommons.org/licenses/by/4.0/).

Any further distribution of this work must maintain attribution to the author(s) and the title of the work, journal citation and DOI.



Jirawat Tangpanitanon<sup>1,2,3,12,\*</sup>, Supanut Thanasilp<sup>1,4,5,12,\*</sup> , Marc-Antoine Lemonde<sup>1,6</sup>, Ninnat Dangniam<sup>5,7,8,9</sup> and Dimitris G Angelakis<sup>1,10,11,\*</sup>

- <sup>1</sup> Centre for Quantum Technologies, National University of Singapore, 3 Science Drive 2 117543, Singapore
  - <sup>2</sup> Quantum Technology Foundation (Thailand), Bangkok, Thailand
  - <sup>3</sup> Thailand Center of Excellence in Physics, Ministry of Higher Education, Science, Research and Innovation, Bangkok, Thailand
  - <sup>4</sup> Institute of Physics, Ecole Polytechnique Fédérale de Lausanne (EPFL), CH-1015 Lausanne, Switzerland
  - <sup>5</sup> Chula Intelligent and Complex Systems, Department of Physics, Faculty of Science, Chulalongkorn University, Bangkok 10330, Thailand
  - <sup>6</sup> Nord Quantique, P1-ACET 3000 Blvd Université, Sherbrooke, Qc J1K 0A5, Canada
  - <sup>7</sup> Department of Physics and Center for Field Theory and Particle Physics, Fudan University, Shanghai 200433, People's Republic of China
  - <sup>8</sup> State Key Laboratory of Surface Physics, Fudan University, Shanghai 200433, People's Republic of China
  - <sup>9</sup> The Institute for Fundamental Study (IF), Naresuan University, Phitsanulok 65000, Thailand
  - <sup>10</sup> School of Electrical and Computer Engineering, Technical University of Crete, Chania 73100, Greece
  - <sup>11</sup> AngelQ Quantum Computing, 531A Upper Cross Street, 04-95 Hong Lim Complex 051531, Singapore
  - <sup>12</sup> The first two authors contributed equally.
- \* Authors to whom any correspondence should be addressed.

E-mail: [jirawat@qtft.org](mailto:jirawat@qtft.org), [supanut.thanasilp@u.nus.edu](mailto:supanut.thanasilp@u.nus.edu) and [dimitris.angelakis@qubit.org](mailto:dimitris.angelakis@qubit.org)

**Keywords:** analog quantum simulators, thermalization, driven quantum many-body systems, quantum supremacy, sampling quantum advantage, random matrix ensembles

## Abstract

A crucial milestone in the field of quantum simulation and computation is to demonstrate that a quantum device can perform a computation task that is classically intractable. A key question is to identify setups that can achieve such goal within current technologies. In this work, we provide formal evidence that sampling bit-strings from a periodic evolution of a unitary drawn from the circular orthogonal ensemble (COE) cannot be efficiently simulated with classical computers. As the statistical properties of COE coincide with a large class of driven analog quantum systems thanks to the Floquet eigenstate thermalization hypothesis, our results indicate the possibility that those driven systems could constitute practical candidates for a sampling quantum advantage. To further support this, we give numerical examples of driven disordered Ising chains and 1D driven Bose–Hubbard model.

## 1. Introduction

A quantum computational advantage is the ability of quantum devices to efficiently perform certain tasks that cannot be efficiently done on a classical computer [1, 2]. Early proposals for realizing this include boson sampling [3–5] and random quantum circuits [6–8]. In both cases, the computational hardness stems from the inability of a classical computer to efficiently sample the output probabilities of a complex quantum evolution. Experimental efforts towards achieving a sampling quantum advantage include optical networks for boson sampling [9–16] and superconducting circuits for random circuits [17–19].

On the other hand, analog quantum simulators are controllable quantum platforms specifically built to implement complex quantum many body models [20–23]. In these experiments, complex quantum dynamics have been implemented which cannot be reproduced with existing classical numerics and have shed light on important questions in quantum many-body physics [24]. However, rigorous proof of a quantum advantage involving complexity theory in those analog systems is limited to specific models such as

the 2D quantum Ising [25, 26] and the 2D cluster-state models [27]. A natural question to ask is: would it be possible to make a complexity statement not only on a particular model but on an entire class of analog quantum systems e.g. when they are in the same quantum phase?

When generic isolated quantum many-body systems thermalize in the sense that any observables can be obtained from the microcanonical ensemble, they share the same statistical properties with random matrix ensembles [28, 29]. One then can expect to gain some insight about the complexity of the thermalized quantum systems by analyzing an evolution of their respective random matrix ensembles.

In this work, we provide strong evidence that sampling from a periodic evolution generated by an instance drawn from a circular orthogonal ensemble (COE) cannot be performed efficiently with a classical computer. Our analysis is based on the absence of collapse of the polynomial hierarchy and a plausible assumption of the worst- to average-case hardness of the sampling task. As indicated by the Floquet eigenstate thermalization hypothesis (ETH), COE is an underlying random matrix ensemble for periodically-driven quantum many-body systems in the thermalized phase [28, 29]. Hence, our findings suggest the possibility that sampling from those thermalized driven quantum systems is also a classically intractable task. We further support the link between COE and the thermalized driven quantum systems by numerically examining specific examples of disordered quantum Ising chain driven by a global magnetic field and the one-dimensional Bose–Hubbard (BH) model with modulated hoppings. As periodically driven systems have been implemented experimentally with current available quantum hardware [17, 30–36], this makes our work also a broad interest to the experimental community. Recently, sampling from a driven thermalized BH model has been experimentally implemented with an ultra-cold atom platform up to 32 sites and 20 atoms [37].

## 2. Framework

### 2.1. Driven analog quantum systems and Floquet ETH

Let us consider a generic periodically-driven quantum many-body system whose Hamiltonian is described by  $\hat{H}(t) = \hat{H}_0 + f(t)\hat{V}$ . Here  $\hat{H}_0$  is the undriven Hamiltonian,  $\hat{V}$  is the driving Hamiltonian such that  $[\hat{H}_0, \hat{V}] \neq 0$ , and  $f(t)$  is periodic with period  $T$ . We require that the time-averaged Hamiltonian  $\hat{H}_{\text{ave}} = \frac{1}{T} \int_0^T \hat{H}(t) dt$  describes an interacting many-body system [38].

Let  $\mathcal{Z} = \{|\mathbf{z}\rangle = \otimes_i^L |z_i\rangle\}$  be a complete basis of many-body Fock states, where  $z_i = \{0, 1, 2, \dots, D_i - 1\}$  denotes the basis state of a local quantum system of dimension  $D_i$  and where  $i \in [1, L]$ . In what follows, we assume without loss of generality that  $D_i = D$  for all  $i$ , resulting in a Hilbert space of dimension  $N = D^L$ . The state after  $M$  driving periods is  $|\psi_M\rangle = \hat{U}_F^M |\mathbf{z}_0\rangle$ , where  $\hat{U}_F = \hat{\mathcal{T}} \exp\left(-i \int_0^T \hat{H}(t) dt\right) \equiv \exp(-i\hat{H}_F T)$  and  $\hat{\mathcal{T}}$  is the time-ordering operator. We assume that the initial state  $|\mathbf{z}_0\rangle$  is a product state. The effective time-independent Floquet Hamiltonian  $\hat{H}_F$  fully describes the dynamics probed at stroboscopic times  $t = nT$ . The probability of measuring the Fock state  $|\mathbf{z}\rangle$  is then  $p_M(\mathbf{z}) = |\langle \mathbf{z} | \psi_M \rangle|^2$  with

$$\langle \mathbf{z} | \psi_M \rangle = \sum_{\mathbf{z}_1, \dots, \mathbf{z}_{M-1} \in \mathcal{Z}} \prod_{m=0}^{M-1} \langle \mathbf{z}_{m+1} | \hat{U}_F | \mathbf{z}_m \rangle, \quad (1)$$

where the sum is performed over  $M - 1$  complete sets of basis states. More precisely, the set of basis states  $\{|\mathbf{z}_m\rangle\}$  is associated with the quantum evolution after  $m$  driving cycles with  $\mathbf{z}_0$  ( $\mathbf{z}_M = \mathbf{z}$ ) being the initial (readout) configuration. The expression in equation (1) can be viewed as the Feynman's path integral where each trajectory is defined by a set of configurations  $\{\mathbf{z}_0, \mathbf{z}_1, \dots, \mathbf{z}_M\}$ . If  $\hat{U}_F$  reaches a required level of randomness, there are many random Feynman trajectories that are equally important, leading to the hardness in calculating the output probability of equation (1).

The ETH states that generic isolated many-body quantum systems thermalize by their own dynamics after a long enough time, regardless of their initial state. In that case, any generic observable is expected to evolve toward the canonical ensemble with a finite temperature [28]. For driven quantum many-body systems, it has been shown that not only thermalization still occurs, but that for low-frequency driving, the associated temperature becomes infinite [29]. In this limit, the Floquet operator  $\hat{U}_F$  shares the statistical properties of the COE. This is an ensemble of matrices whose elements are independent normal complex random variables subjected to the orthogonality and the unitary constraints.

As directly analyzing a complexity of  $\hat{U}_F$  without further specifying structures of the systems is challenging, in this work we attempt to gain some insight from studying COE dynamics. Particularly,  $\hat{U}_F$  in equation (1) is replaced with  $\hat{U}_{\text{COE}}$  where  $\hat{U}_{\text{COE}}$  is a unitary randomly drawn from COE. Even though valuable information can be obtained from the study of COE dynamics, there is a crucial difference between  $\hat{U}_F$  and  $\hat{U}_{\text{COE}}$  due to local structures of the physical systems. Hence, one has to be careful about the

implication of these results for periodically driven systems in the thermalized phase (see section 4 for more discussion).

## 2.2. Sampling quantum advantage

We first introduce a standard procedure used to prove a quantum advantage in quantum random sampling [39]. To understand the computational task, we first define some essential terms used in the complexity theory, namely *approximating*, *sampling*, *multiplicative error* and *additive error*. Let us imagine an analog quantum device built to mimic the quantum dynamics that would lead to  $p_M(\mathbf{z}) = |\langle \mathbf{z} | \psi_M \rangle|^2$ . In practice, such device will encode an output probability  $q(\mathbf{z})$  that differs from  $p_M(\mathbf{z})$  due to noise, decoherence and imperfect controls. Both probabilities are said to be multiplicatively close if

$$|p_M(\mathbf{z}) - q(\mathbf{z})| \leq \alpha p_M(\mathbf{z}) \quad (2)$$

where  $\alpha \geq 0$ . The task of *approximating*  $p_M(\mathbf{z})$  up to *multiplicative error* is to calculate  $q(\mathbf{z})$  that satisfies the above equation for a given  $\mathbf{z}$ . However, such degree of precision is difficult to achieve experimentally as the allowed error is proportional to  $p_M(\mathbf{z})$  which can be much smaller than unity. A more feasible task is to *approximate*  $p_M(\mathbf{z})$  up to *additive error*, defined as

$$\sum_{\mathbf{z} \in \mathcal{Z}} |p_M(\mathbf{z}) - q(\mathbf{z})| \leq \beta, \quad (3)$$

with  $\beta > 0$ . Note that the additive error involves summing over all possible output strings  $\mathbf{z} \in \mathcal{Z}$ , while the multiplicative condition applies to each  $\mathbf{z}$  individually.

The task of *approximating*  $p_M(\mathbf{z})$  even with additive error is still unrealistic as it requires a number of measurements that grows exponentially with the size of the system. What a quantum device can do is to sample strings from  $q(\mathbf{z})$ . Hence, we define the task of *sampling from*  $p_M(\mathbf{z})$  up to *additive error* as generating strings from  $q(\mathbf{z})$  while  $q(\mathbf{z})$  is additively close to  $p_M(\mathbf{z})$ . This task is our central focus to show a sampling quantum advantage. We emphasize that it is different from ‘certifying quantum advantage’ [40] which consists of certifying if equation (3) holds.

To show that the above sampling task cannot be done efficiently by a classical computer, we follow the standard argument which proceeds as follows. Let us suppose that there is a classical machine  $\mathcal{C}$  able to *sample from*  $p_M(\mathbf{z})$  up to *additive error* and that the distribution of  $p_M(\mathbf{z})$  anti-concentrates, i.e.

$$\Pr \left( p_M(\mathbf{z}) > \frac{\delta}{N} \right) \geq \gamma, \quad (4)$$

for some positive constants  $\delta, \gamma > 0$  for all  $\mathbf{z} \in \mathcal{Z}$  [41]. The Stockmeyer theorem states that, with the help of a NP oracle, that machine  $\mathcal{C}$  can also *approximate*  $p_M(\mathbf{z})$  up to *multiplicative error* for some outcomes  $\mathbf{z}$  [39, 42]. We emphasize that the *sampling* task is converted to the *approximation* task in this step. If the latter is #P-hard, then the existence of that machine  $\mathcal{C}$  would imply the collapse of the polynomial hierarchy to the third level, which is strongly believed to be unlikely in computer science. Hence, assuming that the polynomial hierarchy does not collapse to the third level, we reach the conclusion that a classical machine  $\mathcal{C}$  does not exist.

## 3. Sampling from COE dynamics is classically intractable

In this section, we analytically show that sampling up to additive error from a periodic evolution of an instance drawn from COE is classically intractable. The two fundamental conditions of the proof, that is the #P-hardness of *approximating*  $\tilde{p}_M(\mathbf{z})$  up to *multiplicative error* and the anti-concentration of  $\tilde{p}_M(\mathbf{z})$ , are formally stated in the two following theorems.

**Theorem 1 (Worst-case hardness).** *Let  $\mathcal{Y}$  be a set of output probabilities  $\tilde{p}_M(\mathbf{z}) = |\langle \mathbf{z} | \hat{U}_{\text{COE}}^M | \mathbf{z}_0 \rangle|^2$  obtained from all possible COE matrices  $\{\hat{U}_{\text{COE}}\}$  and all possible output strings  $\mathbf{z} \in \mathcal{Z}$ . Approximating  $\tilde{p}_M(\mathbf{z})$  in  $\mathcal{Y}$  up to multiplicative error is #P hard in the worst case.*

**Theorem 2 (Anti-concentration).** *The distribution of  $\tilde{p}_M(\mathbf{z})$  in  $\mathcal{Y}$  anti-concentrates with  $\delta = 1$  and  $\gamma = 1/e$ , where  $e$  is the base of the natural logarithm.*

In theorem 1, we introduced the key notion of *worst-case hardness* of the entire set of COE matrices  $\{\hat{U}_{\text{COE}}\}$ . This corresponds to the scenario where at least one instance  $\tilde{p}_M(\mathbf{z})$ , i.e. a single unitary  $\hat{U} \in \{\hat{U}_{\text{COE}}\}$  and a single configuration  $\mathbf{z} \in \mathcal{Z}$ , is hard to approximate with multiplicative error.

More desirable is the *average-case* hardness where most instances are hard. Consequently, to ensure that the hard instance in  $\mathcal{Y}$  can be found within  $\{\hat{U}_{\text{COE}}\}$  we further assume the following commonly used conjecture which leads to the worst-to-average case reduction in  $\mathcal{Y}$ .

**Conjecture 1 (Average-case hardness).** *For any  $1/2e$  fraction of  $\mathcal{Y}$ , approximating  $\tilde{p}_M(\mathbf{z})$  up to multiplicative error with  $\alpha = 1/4 + o(1)$  is as hard as the hardest instance. Here  $o(\cdot)$  is the little- $o$  notation.*

In combination of theorems 1 and 2 and the conjecture finally allow us to state the main theorem.

**Main Theorem.** *Assuming conjecture 1, the ability to classically sample from  $\tilde{p}_M(\mathbf{z})$  up to an additive error  $\beta = 1/8e$  for all unitary matrices in  $\{\hat{U}_{\text{COE}}\}$  implies the collapse of the polynomial hierarchy to the third level.*

In what follows, we address in detail the proofs of theorems 1 and 2 while the detailed application of the standard Stockmeyer argument to prove the main theorem is provided in appendix A.

### 3.1. #P hardness of simulating COE dynamics

To prove theorem 1, we first notice that the COE is an ensemble of all orthogonal unitary matrices. This includes the well-known instantaneous quantum polynomial (IQP) circuits  $\hat{U}_{\text{IQP}} = \hat{\mathcal{H}}\hat{\mathcal{Z}}\hat{\mathcal{H}}$ , where  $\hat{\mathcal{H}}$  consists of Hadamard gates and  $\hat{\mathcal{Z}}$  is an arbitrary (possibly non-local) diagonal gate on the computational basis, both acting on all qubits [6]. The IQP circuits constitute one of the early proposals of quantum supremacy. Multiplicative approximation of their output probabilities are known to be #P-hard in the worst case [43, theorem 1.4]. Since  $\hat{U}_{\text{IQP}}^M = \hat{\mathcal{H}}\hat{\mathcal{Z}}^M\hat{\mathcal{H}}$  still adopt the general form of the IQP circuits, we conclude that there exists at least one instance in  $\mathcal{Y}$  that is #P-hard for multiplicative approximation.

To see how the hardness could emerge for a typical instance in  $\mathcal{Y}$  (conjecture 1), one can in principle map the path integral in equation (1) to the partition function of a classical Ising model with random complex fields. The latter is widely conjectured to be #P-hard on average for multiplicative approximation [25, 44]. In this context, the key is to note that a COE unitary evolution can be written as  $\hat{U}_{\text{COE}} = \hat{U}_{\text{CUE}}^T \hat{U}_{\text{CUE}}$ , where  $\hat{U}_{\text{CUE}}$  is a random matrix drawn from the circular unitary ensemble (CUE), i.e. the ensemble of Haar-random matrices [45]. Furthermore,  $\hat{U}_{\text{CUE}}$  can be decomposed into a set of universal quantum gates which can be mapped onto a complex Ising model. This mapping procedure has already been described in [7] to support the conjecture of the worst-to-average case in the context of random quantum circuits. A detailed and intuitive description of this protocol is presented in appendix B. Importantly, appendix B shows that, despite the time-reversal symmetry from COE dynamics, approximating the partition function of such mapped Ising model is still #P-hard.

### 3.2. Anti-concentration of COE dynamics

To prove the second and necessary ingredient of the proof, i.e. theorem 2, we write

$$\langle \mathbf{z} | \hat{U}_{\text{COE}}^M | \mathbf{z}_0 \rangle = \sum_{\epsilon=0}^{N-1} d_{\epsilon}(\mathbf{z}) e^{i\phi_{M,\epsilon}}, \quad (5)$$

where  $d_{\epsilon}(\mathbf{z}) = \langle \mathbf{z} | E_{\epsilon} \rangle \langle E_{\epsilon} | \mathbf{z}_0 \rangle$ ,  $\phi_{M,\epsilon} = ME_{\epsilon} T \bmod 2\pi$ ,  $|E_{\epsilon}\rangle$  is an eigenstate of  $\hat{H}_F$  with eigenenergy  $E_{\epsilon}$ . For COE operators,  $d_{\epsilon}(\mathbf{z})$  are real [45] and their distribution, denoted as  $\text{Pr}(d)$ , is given by the Bessel function of the second kind (see figure 1(a) and appendix C for a detailed derivation). Consequently, the values of  $d_{\epsilon}(\mathbf{z})$  for different  $\epsilon$  and  $\mathbf{z}$  do not concentrate on a particular value.

Now let us consider the statistics of the phases  $\{\phi_{M,\epsilon}\}$ . We define the level spacing as  $r_{\epsilon} = \min(\delta_{\epsilon+1}, \delta_{\epsilon}) / \max(\delta_{\epsilon+1}, \delta_{\epsilon})$  with  $\delta_{\epsilon} = \phi_{\epsilon+1} - \phi_{\epsilon} > 0$ . For a single driving cycle  $M = 1$ , the phases  $\{\phi_{1,\epsilon}\}$  for COE are known to exhibit phase repulsion, i.e. the phases are correlated [29]. The COE distribution  $\text{Pr}_{\text{COE}}(r_{\epsilon})$  is depicted in figure 1(b), where  $\text{Pr}_{\text{COE}}(0) = 0$  explicitly indicates the phase repulsion. For multiple driving cycles  $M \gg 2\pi/E_{\epsilon}T$ , the correlations are erased due to energy folding, i.e. the effect of the modulo  $2\pi$ . This results in the Poisson (POI) distribution of the level spacing,  $\text{Pr}_{\text{POI}}(r_{\epsilon}) = 2/(1+r_{\epsilon}^2)$ , with the peak at  $r = 0$ , see figure 1(b).

The Bessel function distribution of  $d_{\epsilon}(\mathbf{z})$  and the POI distribution of  $\phi_{M,\epsilon}$  ensure that the output distribution  $\text{Pr}(p)$  is not concentrated. Specially,  $\text{Pr}(p)$  follows the so-called Porter-Thomas distribution

$$\text{Pr}_{\text{PT}}(p) = N e^{-Np}, \quad (6)$$

for  $N \gg 1$ . The presence of the Porter-Thomas distribution suggests that the system uniformly explores the Hilbert space [17, 25]. In [46], it has been shown that the quantum system that follows the Porter-Thomas distribution also thermalizes to infinite temperature. As the temperature associated with driven thermalized

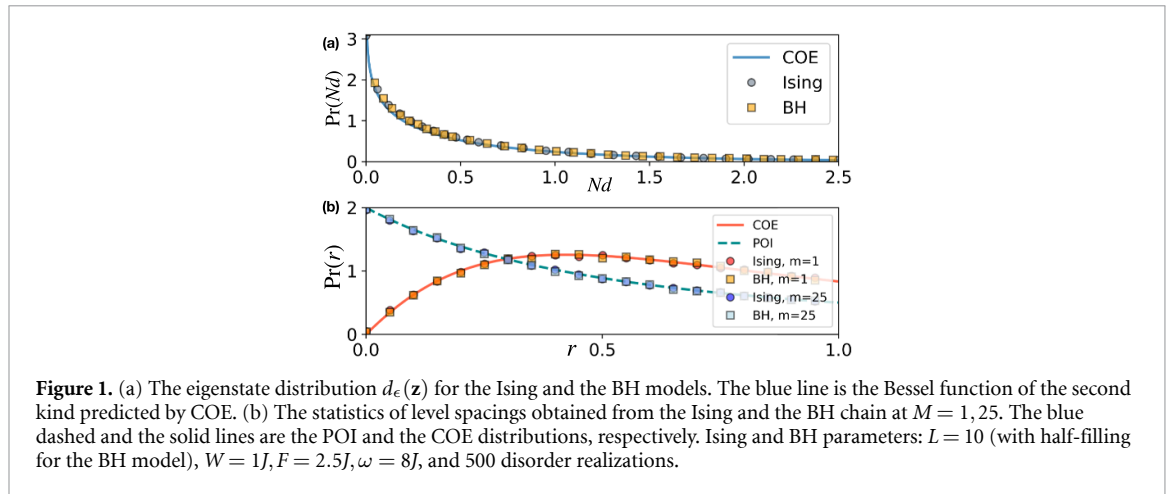


**Figure 1.** (a) The eigenstate distribution  $d_\epsilon(\mathbf{z})$  for the Ising and the BH models. The blue line is the Bessel function of the second kind predicted by COE. (b) The statistics of level spacings obtained from the Ising and the BH chain at  $M = 1, 25$ . The blue dashed and the solid lines are the POI and the COE distributions, respectively. Ising and BH parameters:  $L = 10$  (with half-filling for the BH model),  $W = 1J, F = 2.5J, \omega = 8J$ , and 500 disorder realizations.

phase is infinite, this highlights the importance of the drive in the protocol. In addition, the Porter-Thomas distribution also appears from the quantum random circuits and can be seen as one of the key signatures of the sampling quantum advantage [7, 17, 25]. Above all, the most important role played by the Porter-Thomas distribution in the sampling quantum advantage is that it satisfies the anti-concentration condition. This is since  $\text{Pr}_{\text{PT}}(p > \frac{1}{N}) = \int_{Np=1}^{\infty} d(Np)e^{-Np} = 1/e$ , indicating that most of possible outcomes (e.g. bit-strings) have non-zero probabilities of being measured [7].

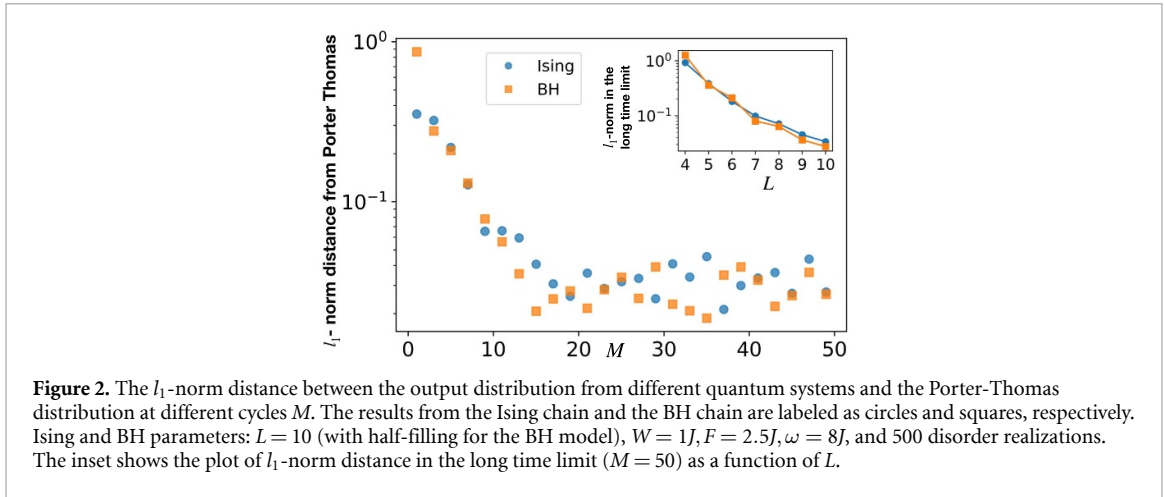
To see the emergence of the Porter-Thomas distribution in the COE dynamics, we write  $\langle \mathbf{z} | \psi_M \rangle = a_{\mathbf{z}} + ib_{\mathbf{z}}$ , where  $a_{\mathbf{z}} = \sum_{\epsilon} d_{\epsilon}(\mathbf{z}) \cos \phi_{M,\epsilon}$  and  $b_{\mathbf{z}} = \sum_{\epsilon} d_{\epsilon}(\mathbf{z}) \sin \phi_{M,\epsilon}$ . Due to the Poisson distribution in the long time limit, the phases  $\{\phi_{M,\epsilon}\}$  can be thought of as independent variables randomly and uniformly distributed in the range  $[0, 2\pi)$ . Using the product distribution formula and the central limit theorem, one can show that the distributions of  $a_{\mathbf{z}}$  and  $b_{\mathbf{z}}$  are normal distributions with zero mean and variance  $1/2N$ . Since  $\tilde{p}_M(\mathbf{z}) = a_{\mathbf{z}}^2 + b_{\mathbf{z}}^2$ , the Porter-Thomas distribution of  $\tilde{p}_M(\mathbf{z})$  can be derived using the fact that the square sum of two Gaussian variables follows the  $\chi$ -squared distribution with second degree of freedom [47]. A detailed derivation is presented in appendix C.

#### 4. Implications of COE hardness for driven thermalized systems

Here we discuss implication of our results obtained in the previous section for the periodically driven quantum many-body systems when they thermalize. As the driven thermalized quantum systems and COE are closely related through the Floquet ETH, the absence of efficient classical algorithms to classically sample form COE dynamics suggests the possibility that the same result also holds for the generic thermalized driven quantum systems. Physically, this is due to the external periodic drive boosting the level of randomness [48, 49]. A more detailed analysis of  $\hat{H}_F$  using Magnus expansion shows that the presence of low-frequency driving allows to generate effective infinite-range multi-body interactions [29, 50]. Therefore lifting most of the constraints imposed by the limited local few-body interactions generally encountered in physical systems. This is in contrast to the case of generic *undriven* thermalized systems. In that context, accurate descriptions of the systems using random matrix theory is in general only possible over small energy windows far from the energy-spectrum edges. If one analyses the entire energy spectrum, the local structure typically encountered in static Hamiltonians emerges and random matrix theory fails to capture it. This is not the case for driven thermalized systems which accurately applies to the entire  $\hat{U}_F$  spectrum. Furthermore, under the condition that COE and the driven thermalized systems share the same statistical distributions as indicated by the Floquet ETH, the anti-concentration result (Theorem 2) is readily applicable to the driven thermalized quantum systems.

Nevertheless, we emphasize here that one should not interpret our results as a formal proof of a sampling quantum advantage in the generic driven thermalized quantum systems, but rather as an indication to support the statement. This is due to the fact that, albeit sharing the same statistics, the Floquet unitary is unlikely to be a typical COE instance. Lastly, our discussion here only applies to the periodically driven systems when they *already* thermalize. There are other phases and regimes such as a many-body localized phase [51] and a prethermalized regime [52] which we do not consider here. Though, we note that the sampling complexity of the generic MBL phase has been proven to be classically efficient [46].





#### 4.1. Example of driven thermalized many-body systems

We give two specific examples of driven systems that display statistical properties consistent with the COE and are able to reach the Porter-Thomas distribution with a polynomial number of cycles, hence partially support our suggestion of a sampling quantum advantage. For both cases, the modulation is

$f(t) = \frac{1}{2}(1 - \cos(\omega t))$ , where  $\omega = 2\pi/T$  and initial states are randomized product states.

(i) 1D Ising chain: We consider an Ising chain described by the Hamiltonian  $\hat{H}_0^{\text{ISING}} = \sum_{l=0}^{L-1} \mu_l \hat{Z}_l + J \sum_{l=0}^{L-2} \hat{Z}_l \hat{Z}_{l+1}$ , where  $\mu_l \in \{0, W\}$  is a local disorder,  $W$  is the disorder strength,  $\hat{Z}_l$  is the Pauli spin operator acting on site  $l$ , and  $J$  is the interaction strength. The drive is a global magnetic field  $\hat{V}^{\text{ISING}} = F \sum_{l=0}^{L-1} \hat{X}_l$ , where  $F$  is the driving amplitude. Similar models have been implemented in various quantum platforms, including trapped ions [33] and superconducting circuits [34].

(ii) 1D BH model: We consider the BH model described by the Hamiltonian  $\hat{H}_0^{\text{BH}} = \sum_{l=0}^{L-1} (\mu_l \hat{a}_l^\dagger \hat{a}_l + \frac{U}{2} \hat{a}_l^\dagger \hat{a}_l^\dagger \hat{a}_l \hat{a}_l)$ , where  $\hat{a}_l$  ( $\hat{a}_l^\dagger$ ) is a bosonic annihilation (creation) operator at site  $l$ ,  $U$  is the on-site interaction, and  $\mu_l$  is the local disorder as defined above. The drive modulates the hopping amplitudes  $\hat{V}^{\text{BH}} = -F \sum_{l=0}^{L-2} (\hat{a}_l^\dagger \hat{a}_{l+1} + \text{H.c.})$ . Similar models have been implemented in superconducting circuits [17] and cold atoms [30, 32, 35].

The distribution of  $d_\epsilon(\mathbf{z})$  from both models are depicted in figure 1(a), showing an agreement with the Bessel function as predicted by COE. The level statistics at  $M = 1$  and  $M = 25$  are depicted in figure 1(b), showing an agreement with the COE and the POI distribution, respectively. The driving frequency and the disorder strength are tuned to ensure the observation of the thermalized phase and prevent many-body localization [29, 46].

Figure 2 shows the  $l_1$ -norm distance between  $\text{Pr}(p)$  and the Porter-Thomas distribution at different  $m$  for the Ising and the BH models. The  $l_1$ -norm distance measures the difference between two distributions and only becomes zero only when they are identical. It can be seen that, in all cases, the system reaches the Porter-Thomas distribution after multiple driving cycles. The  $l_1$ -norm distance in the long-time limit is decaying towards zero as the size of the system increases. Therefore, the anti-concentration condition is satisfied. In addition, the drive induces the effectively infinite long-range interactions in the Floquet Hamiltonian. Consequently, we expect the driven thermalized quantum systems to achieve the Porter-Thomas distribution in the faster time scale compared to the quantum random circuits with the same topology. This aspect has been studied numerically in [46].

In absence of the drive, a similar analysis can be performed for the infinite-time unitary evolution corresponding to generic instances of the undriven thermalized phase in both models. In this case,  $d_\epsilon(\mathbf{z})$  does not follow the Bessel function of the second kind and the output distribution never reaches the Porter-Thomas distribution (see appendix D for numerical simulation of the undriven Ising model). This is consequence of the energy conservation and the structure imposed by the local interactions, highlighting the key role played by the drive. We note here that the choice of  $l_1$ -norm in figure 2 as the distinguishability measure between two distribution is due to its key role in the proof of the sampling quantum advantage. However, other distinguishability measures can also be used in this numeric. Particularly, KL-divergence has been used to measure the difference from the Porter-Thomas distribution in [17, 46, 53].

Lastly, we note that the proposal to sample from a driven thermalized quantum system has been implemented in practice with the ultra-cold atom platform [37]. In this experiment, sampling one sample from driven thermalized BH model requires around 500 seconds. In comparison, estimated time of around

$10^4$  seconds and classical memory of around 600 TB are required to generate one sample on Frontier supercomputer using exact diagonalization.

## 5. Conclusion and outlook

Analog quantum simulators realizing quantum many-body systems have generated quantum dynamics beyond the reach of existing classical numerical methods for some time. However, such dynamics has not been theoretically proven to be hard to compute by a classical computer. We have taken the first step into proving that in the particular case of driven many-body systems, when they thermalize, sampling from their output distribution cannot be efficiently performed on a classical computer. Using complexity theory arguments, we provide strong analytical evidence of the computational hardness of sampling from the COE dynamics. As a consequence, the same complexity result might be expected for the driven thermalized quantum systems thanks to their closed link with COE. We further argue that this possibility is much more likely to happen in the driven case compared to the undriven one as more randomness added into the systems due to the external drive. We provide numerical results showing that COE statistics and reaching the Porter-Thomas distribution with polynomially many cycles can be obtained from driven quantum Ising and BH models for realistic parameters.

All together, our results pave the way to realize a sampling quantum advantage of analog quantum simulators with currently available platforms, including trapped ions and cold atoms [33, 36]. In the future, the next important step is to analyze complexity of a specific model in driven thermalization, such as driven Ising spin chains, and demonstrate a sampling quantum advantage directly from the physical system. In addition, it would be interesting to see at what extent one can probe the complexity of physical systems from their respective matrix ensembles. For example, whether this approach can be extended to other classes of quantum many-body systems such as those with gauge fields or frustrated systems.

## Data availability statement

The data generated and/or analyzed during the current study are not publicly available for legal/ethical reasons but are available from the corresponding author on reasonable request.

## Acknowledgment

This research is supported by the National Research Foundation, Singapore and A\*STAR under its CQT Bridging Grant and Quantum Engineering Programme NRF2021-QEP2-02-P02, and by EU HORIZON—Project 101080085 – QCFD. It was also partially funded by Polisimulator project co-financed by Greece and the EU Regional Development Fund. Ninnat Dangniam is supported by the National Natural Science Foundation of China (Grant No. 11875110). Additionally, Ninnat Dangniam and Supanut Thanasilp are partially supported by Thailand Science Research and Innovation Fund Chulalongkorn University (IND66230005).

## Appendix A. Proof of the main theorem

In this section, we provide a detailed proof of the main theorem of the main text, which reads:

**Main Theorem.** *Assuming conjecture 1, the ability to classically sample from  $\tilde{p}_M(\mathbf{z})$  up to an additive error  $\beta = 1/8e$  for all unitary matrices in  $\{\hat{U}_{\text{COE}}\}$  implies the collapse of the polynomial hierarchy to the third level.*

The proof relies on the theorems 1 and 2 and conjecture 1 presented in the main text.

**Theorem 1.** *Let  $\mathcal{Y}$  be a set of output probabilities  $\tilde{p}_M(\mathbf{z}) = |\langle \mathbf{z} | \hat{U}_{\text{COE}}^M | \mathbf{z}_0 \rangle|^2$  obtained from all possible COE matrices  $\{\hat{U}_{\text{COE}}\}$  and all possible output strings  $\mathbf{z} \in \mathcal{Z}$ . Approximating  $\tilde{p}_M(\mathbf{z})$  in  $\mathcal{Y}$  up to multiplicative error is  $\#\text{P}$  hard in the worst case.*

**Theorem 2.** *The distribution of  $\tilde{p}_M(\mathbf{z})$  in  $\mathcal{Y}$  anticoncentrates with  $\delta = 1$  and  $\gamma = 1/e$ , where  $e$  is the base of the natural logarithm.*

**Conjecture 1 (Average-case hardness).** *For any  $1/(2e)$  fraction of  $\mathcal{Y}$  approximating  $\tilde{p}_M(\mathbf{z})$  up to multiplicative error with  $\alpha = 1/4 + o(1)$ , where  $o(\cdot)$  is little-o notation [54], is as hard as the hardest instance.*

Let us begin by considering a classical probabilistic computer with an NP oracle, also called a  $\text{BPP}^{\text{NP}}$  machine. This is a theoretical object that can solve problems in the third level of the polynomial hierarchy.



The Stockmeyer theorem states that a BPP<sup>NP</sup> machine with an access to a classical sampler  $\mathcal{C}$ , as defined in the main text, can efficiently output an approximation  $\tilde{q}(\mathbf{z})$  of  $q(\mathbf{z})$  such that

$$|q(\mathbf{z}) - \tilde{q}(\mathbf{z})| \leq \frac{q(\mathbf{z})}{\text{poly}(L)}. \tag{A1}$$

We emphasize that the BPP<sup>NP</sup> machine grants us the ability to perform the approximating task, in contrast to the machine  $\mathcal{C}$  that can only sample strings from a given distribution. To see how the BPP<sup>NP</sup> machine can output a multiplicative approximation of  $\tilde{p}_M(\mathbf{z})$  for most of  $\mathbf{z} \in \mathcal{Z}$ , let us consider

$$\begin{aligned} |\tilde{p}_M(\mathbf{z}) - \tilde{q}(\mathbf{z})| &\leq |\tilde{p}_M(\mathbf{z}) - q(\mathbf{z})| + |q(\mathbf{z}) - \tilde{q}(\mathbf{z})| \\ &\leq |\tilde{p}_M(\mathbf{z}) - q(\mathbf{z})| + \frac{q(\mathbf{z})}{\text{poly}(L)} \\ &\leq |\tilde{p}_M(\mathbf{z}) - q(\mathbf{z})| + \frac{|\tilde{p}_M(\mathbf{z}) - q(\mathbf{z})| + \tilde{p}_M(\mathbf{z})}{\text{poly}(L)} \\ &= \frac{\tilde{p}_M(\mathbf{z})}{\text{poly}(L)} + |\tilde{p}_M(\mathbf{z}) - q(\mathbf{z})| \left(1 + \frac{1}{\text{poly}(L)}\right). \end{aligned} \tag{A2}$$

The first and the third lines are obtained using the triangular inequality. To get multiplicative approximation of  $\tilde{p}_M(\mathbf{z})$  using  $\tilde{q}(\mathbf{z})$ , we need the term  $|\tilde{p}_M(\mathbf{z}) - q(\mathbf{z})|$  to be small. Given the additive error defined in equation (3) in the main text, this is indeed the case for a large portion of  $\{\mathbf{z}\} \in \mathcal{Z}$ . Since the left hand side of equation (3) in the main text involves summing over an exponentially large number of terms but the total error is bounded by a constant  $\beta$ , most of the terms in the sum must be exponentially small. This statement can be made precise using Markov’s inequality.

**Fact 1 (Markov’s inequality).** *If  $X$  is a non-negative random variable and  $a > 0$ , then the probability that  $X$  is at least  $a$  is*

$$\Pr(X \geq a) \leq \frac{\mathbb{E}(X)}{a}, \tag{A3}$$

where  $\mathbb{E}(X)$  is the expectation value of  $X$ .

By setting  $X = |\tilde{p}_M(\mathbf{z}) - q(\mathbf{z})|$ , we get

$$\Pr_{\mathbf{z}}(|\tilde{p}_M(\mathbf{z}) - q(\mathbf{z})| \geq a) \leq \frac{\mathbb{E}_{\mathbf{z}}(|\tilde{p}_M(\mathbf{z}) - q(\mathbf{z})|)}{a}. \tag{A4}$$

Here, the distribution and the expectation value are computed over  $\mathbf{z} \in \mathcal{Z}$ . Note that  $\mathbb{E}_{\mathbf{z}}(|\tilde{p}_M(\mathbf{z}) - q(\mathbf{z})|) \leq \beta/N$  is given by the additive error defined in equation (3) in the main text. By setting  $a = \beta/N\zeta$  for some small  $\zeta > 0$ , we get

$$\Pr_{\mathbf{z}}\left(|\tilde{p}_M(\mathbf{z}) - q(\mathbf{z})| \geq \frac{\beta}{N\zeta}\right) \leq \zeta \tag{A5}$$

or equivalently

$$\Pr_{\mathbf{z}}\left(|\tilde{p}_M(\mathbf{z}) - q(\mathbf{z})| < \frac{\beta}{N\zeta}\right) > 1 - \zeta. \tag{A6}$$

By substituting  $|\tilde{p}_M(\mathbf{z}) - q(\mathbf{z})|$  from equation (A2), we get

$$\Pr_{\mathbf{z}}\left(|\tilde{p}_M(\mathbf{z}) - \tilde{q}(\mathbf{z})| < \frac{\tilde{p}_M(\mathbf{z})}{\text{poly}(L)} + \frac{\beta}{N\zeta} \left(1 + \frac{1}{\text{poly}(L)}\right)\right) > 1 - \zeta. \tag{A7}$$

Theorem 2 in the main text (the anti-concentration condition) imply that  $\{\tilde{p}_M(\mathbf{z})\}$  follows the Porter-Thomas distribution, specially that  $1/N < \tilde{p}_M(\mathbf{z})$  for at least  $1/e$  fraction of the unitary matrices in  $\{\hat{U}_{\text{COE}}\}$ . Hence, we can rewrite equation (A7) as

$$\Pr_{\mathbf{y}}\left\{|\tilde{p}_M(\mathbf{z}) - \tilde{q}(\mathbf{z})| < \tilde{p}_M(\mathbf{z}) \left[\frac{1}{\text{poly}(L)} + \frac{\beta}{\zeta} \left(1 + \frac{1}{\text{poly}(L)}\right)\right]\right\} > 1/e - \zeta. \tag{A8}$$

Here, the distribution is over all  $\mathbf{z} \in \mathcal{Z}$  and all unitary matrices in  $\{\hat{U}_{\text{COE}}\}$ . To understand the right hand side of the equation, let  $P \cap Q$  be the intersection between the set  $P$  of probabilities that anticenterate and

the set  $Q$  of probabilities that satisfy the Markov's inequality. Since  $\Pr(P \cap Q) = \Pr(P) + \Pr(Q) - \Pr(P \cup Q) \geq \Pr(P) + \Pr(Q) - 1$ ,  $\Pr(P) = 1/e$  and  $\Pr(Q) = 1 - \zeta$ , it follows that  $\Pr(P \cap Q)$  is no less than  $1/e + 1 - \zeta - 1 = 1/e - \zeta$ .

Following [7, 44], we further set  $\beta = 1/(8e)$  and  $\zeta = 1/(2e)$ , so that

$$\Pr_{\hat{U}_{\text{COE}, \mathbf{z}}} \left\{ |\tilde{p}_M(\mathbf{z}) - \tilde{q}(\mathbf{z})| < \left( \frac{1}{4} + o(1) \right) \tilde{p}_M(\mathbf{z}) \right\} > \frac{1}{2e}, \quad (\text{A9})$$

giving an approximation up to multiplicative error  $1/4 + o(1)$  for at least  $1/(2e)$  instances of the COE matrices  $\{\hat{U}_{\text{COE}}\}$ . If according to the conjecture 1 in the main text, multiplicatively estimating  $1/(2e)$  fraction of the output probabilities from  $\{\hat{U}_{\text{COE}}\}$  is #P-hard, then the Polynomial Hierarchy collapses. This concludes the proof of the main theorem in the main text.

## Appendix B. Mapping of approximating output distribution of COE dynamics onto estimating partition function of complex Ising models

In this section, we provide evidence to support the conjecture 1 in the main text, showing how hardness instances could appear on average. To do this, we map the task of approximating an output distributions of COE dynamics onto calculating the partition function of a classical Ising model which is widely believed to be #P-hard on average for multiplicative approximation [25, 44]. The section is divided into two parts. In the first part, we explain the overall concept and physical intuition of this procedure. In the second part, mathematical details are provided.

### B.1. Physical perspective of the mapping procedure

The mapping protocol consists of two intermediate procedures. First, we map the COE unitary evolution on *universal* random quantum circuits and, second, we derive a complex Ising model from those circuits following [7].

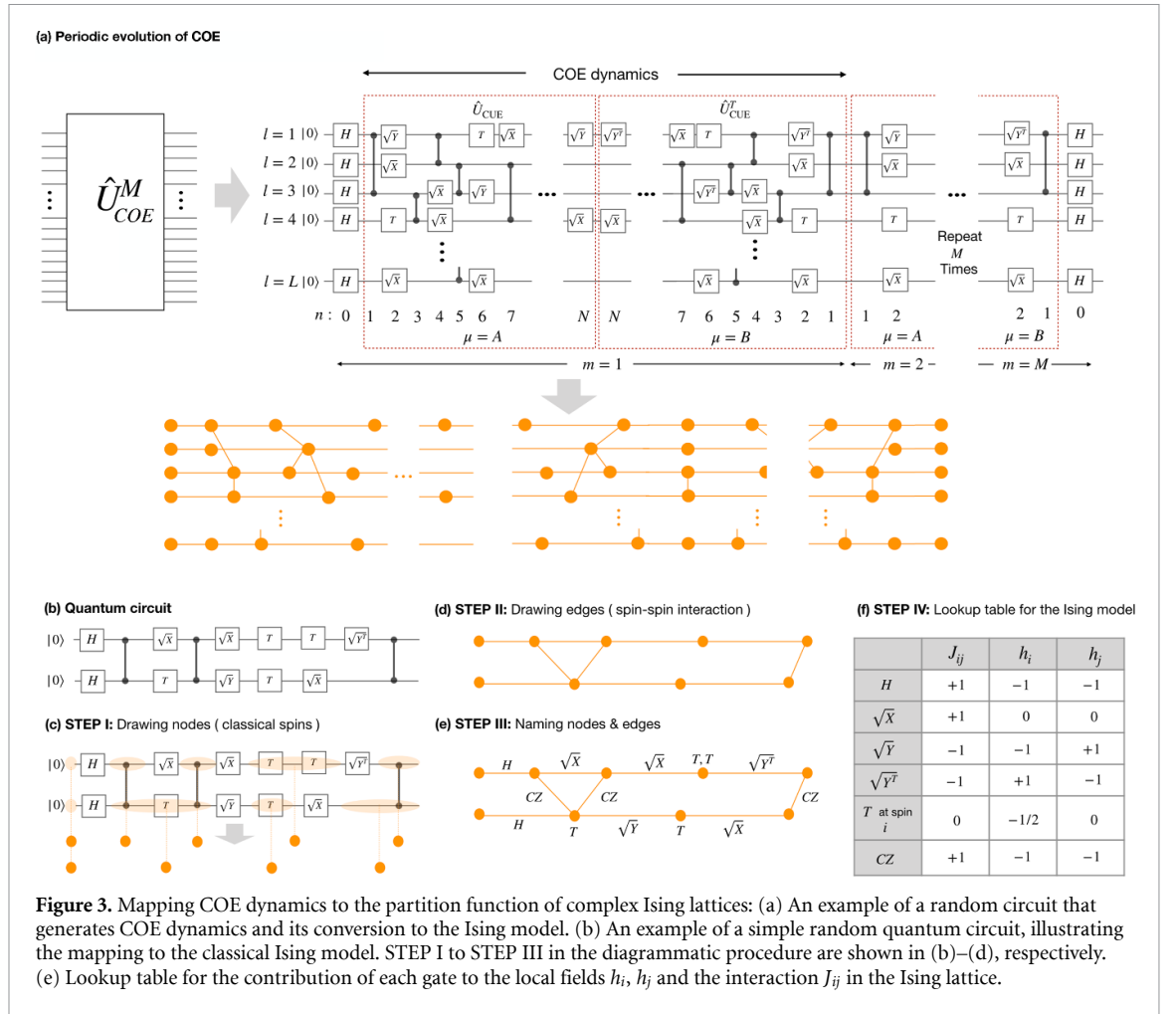
Let us begin by expressing a unitary evolution of COE as  $\hat{U}_{\text{COE}} = \hat{U}_{\text{CUE}}^T \hat{U}_{\text{CUE}}$  where  $\hat{U}_{\text{CUE}}$  is a random unitary drawn from the CUE i.e. Haar ensemble [45]. We then further decompose  $\hat{U}_{\text{CUE}}$  into a set of universal quantum gates [7]. Following [7], we choose random quantum circuits consisting of  $n + 1$  layers of gates and  $\log_2 N$  qubits, as shown in figure 3(a). The first layer consists of Hadamard gates applied to all qubits. The following layers consist of randomly chosen single-qubit gates from the set  $\{\sqrt{X}, \sqrt{Y}, T\}$  and two-qubit controlled-Z (CZ) gates. Here,  $\sqrt{X}$  ( $\sqrt{Y}$ ) represents a  $\pi/2$  rotation around the  $X$  ( $Y$ ) axis of the Bloch sphere and  $\hat{T}$  is a non-Clifford gate representing a diagonal matrix  $\{1, e^{i\pi/4}\}$ . Such circuits have been shown to be approximately  $t$ -design [55] for an arbitrary large  $t$  when  $n \rightarrow \infty$ , which implies the CUE evolution [56]. The operator  $\hat{U}_{\text{CUE}}^T$  can be implemented by reversing the order of the gates in  $\hat{U}_{\text{CUE}}$  and replacing  $\sqrt{Y}$  with  $\sqrt{Y}^T$ . We emphasize that decomposing the COE evolution into the random circuits is only done theoretically with an aim to show the average case hardness. In the real experiments, this COE dynamics is realized by the driven many-body systems.

The mathematical procedure for the mapping from random quantum circuits to classical complex Ising models is discussed in details in the next part. Specifically,  $p_M(\mathbf{z})$  from the circuit  $(\hat{U}_{\text{CUE}}^T \hat{U}_{\text{CUE}})^M$ , as depicted in figure 3(a), can be calculated from the partition function,

$$\langle \mathbf{z} | \hat{U}_{\text{COE}}^M | \mathbf{z}_0 \rangle = \sum_{\mathbf{s} \in \mathcal{S}} A(\mathbf{s}) \exp \left[ \frac{i\pi}{4} \left( \sum_i h_i s_i + \sum_{\langle i, j \rangle} J_{ij} s_i s_j \right) \right]. \quad (\text{B1})$$

Here,  $A(\mathbf{s})$  is the degeneracy number associated with a classical spin configuration  $\mathbf{s}$  in the lattice  $\mathcal{S}$ ,  $s_i = \pm 1$ ,  $h_i$  represents a on-site field on site  $i$  and  $J_{ij}$  represents the coupling between the classical spins on site  $i$  and  $j$ . Since the output probability can also be interpreted as the path integral in equation (B1) in the main text, the intuition behind the mapping is that the sum over all possible paths is translated into the sum over all possible classical spin configurations, where the phase accumulated in each path is given by the energy of the complex Ising lattice  $\mathcal{S}$ . To gain intuitive understanding of this standard mapping, we provide a diagrammatic approach to visualize the lattice  $\mathcal{S}$  and extract the field parameters  $\{h_i\}$ ,  $\{J_{ij}\}$ . To begin with, we use the random circuit in figure 3(b) as a demonstration. The mathematical descriptions behind each steps are discussed in the next part.

- **STEP I**—For each qubit, draw a circle between every consecutive non-diagonal gates, see figure 3(c). Each circle or ‘node’ represents one classical spin.



- **STEP II**—For each qubit, draw a horizontal line between every consecutive nodes  $i, j$ , see figure 3(d). These lines or ‘edges’ represent interaction  $J_{ij}$  between two neighboring spins in the same row. In addition, draw a line between every two nodes that are connected by CZ gates. These lines represent the interaction  $J_{ij}$  between spins in different rows.
- **STEP III**—Labeling each nodes and edges with the corresponding gates, see figure 3(e).
- **STEP IV**—Use the lookup table in figure 3(f) to specify  $h_i$  and  $J_{ij}$  introduced by each gate. For example, the  $\sqrt{Y}$  gate that acts between nodes  $i$  and  $j$  adds  $-1$  to  $J_{ij}$ ,  $-1$  to  $h_i$  and  $+1$  to  $h_j$ . We use the convention that the leftmost index represents the leftmost node. Also, the two T-gates that are enclosed by the node  $i$  will add  $0.5 + 0.5 = +1$  to the local field  $h_i$ .
- **STEP V**—Finally, spins at the leftmost side of the lattice are fixed at  $+1$ , corresponding to the initial state  $|0\rangle$ . Similarly, spins at the rightmost side of the lattice are fixed according to the readout state  $|z\rangle$ .

Following the above recipe in the next part, we provide the exact form of the partition function of the Ising model for the COE dynamics in equation (B19), showing that the field parameters  $\{h_i\}$  and  $\{J_{ij}\}$  are quasi-random numbers with no apparent structure. Specifically, neither the phase  $\pi \sum_i h_i s_i / 4$  nor the phase  $\pi \sum_{\langle i, j \rangle} J_{ij} s_i s_j / 4$  is restricted to the values  $0, \pi/2, \pi, 3\pi/2 \pmod{2\pi}$  for each spin configurations  $\mathbf{s}$ . Without such stringent restrictions, approximating the partition function up to multiplicative error is known to be #P-hard in the worst case [43, theorem 1.9]. This motivates a widely used conjecture in quantum supremacy proposals that such task is also hard on average [25, 44].

We emphasize here the major differences between random quantum circuits as proposed in [7] and our systems. Firstly, our systems are analog with no physical quantum gates involved. The decomposition to quantum gates is only done mathematically. Secondly, our system has discrete time-reversal symmetry, while such symmetry is absent in random quantum circuits. Consequently, the COE in our system is achieved from the Floquet operator  $\hat{U}_F$ , while the CUE in random quantum circuits are achieved from the entire unitary

evolution. In addition,  $\hat{U}_F^M$  in our system does not have the  $t$ -design property due to the COE [57, pp.117-119]. However, as shown above, the hardness arguments for the random quantum circuits can be naturally applied to our case. Therefore, same as the random quantum circuits, approximating the partition function of the mapped Ising model from COE dynamic is also classically intractable in the worst case.

### B.2. Mathematical details of the mapping procedure

In this section, we prove equation (B1) by providing justifications of the diagrammatic recipes to map the evolution  $\hat{U}_{\text{CUE}}$  on a Ising spin model with complex fields. Again, the quantum gates of interest consist of both diagonal gates  $\{T, CZ\}$  and non-diagonal gates  $\{\sqrt{X}, \sqrt{Y}, \sqrt{Y}^T, H\}$ . For simplicity, we start with one- and two- qubit examples before generalizing to the COE dynamics. The mathematical procedure here is adapted from [7].

#### B.2.1. One-qubit example

Let us consider a one-qubit circuit and  $N + 1$  gates randomly chosen from the set  $\{\sqrt{X}, \sqrt{Y}, \sqrt{Y}^T, T\}$ . The zeroth gate is fixed to be a Hadamard gate. The output probability is  $p(z) = |\langle z | \hat{U} | 0 \rangle|^2$ , where  $\hat{U} = \prod_{n=0}^N \hat{U}^{(n)}$  is the total unitary matrix,  $\hat{U}^{(n)}$  is the  $n^{\text{th}}$  gate and  $z \in \{0, 1\}$  is the readout bit. Below, we outline the mathematical steps underlying the diagrammatic approach followed by detailed explanations for each step:

$$\begin{aligned}
 p(z) &= \left| \langle z | \prod_{n=0}^N \hat{U}^{(n)} | 0 \rangle \right|^2 \\
 &= \left| \sum_{\underline{z} \in \{0,1\}^N} \prod_{n=0}^N \langle z_n | \hat{U}^{(n)} | z_{n-1} \rangle \right|^2 \\
 &= \left| \sum_{\underline{z} \in \{0,1\}^N} \prod_{n=0}^N A(z_n, z_{n-1}) \exp \left[ \frac{i\pi}{4} \Phi(z_n, z_{n-1}) \right] \right|^2 \\
 &= \left| \sum_{\underline{z} \in \{0,1\}^{N+2}} A(\underline{z}) \exp \left[ \frac{i\pi}{4} \sum_{n=0}^N \Phi(z_n, z_{n-1}) \right] \right|^2. \tag{B2}
 \end{aligned}$$

In the second line, we insert an identity  $\hat{I}_n = \sum_{z_n \in \{0,1\}} |z_n\rangle\langle z_n|$  between  $\hat{U}^{(n+1)}$  and  $\hat{U}^{(n)}$  for every  $n \in \{0, \dots, N-1\}$ . As a result, this line can be interpreted as the Feynman's path integral where each individual path or 'world-line' is characterized by a sequence of basis variables  $\underline{z} = (z_{-1}, z_0, \dots, z_N)$ . The initial and the end points for every path are  $|z_{-1}\rangle = |0\rangle$  and  $|z_N\rangle = |z\rangle$ , respectively. In the third line, we decompose  $\langle z_n | \hat{U}^{(n)} | z_{n-1} \rangle$  into the amplitude  $A(z_n, z_{n-1})$  and phase  $\Phi(z_n, z_{n-1})$ . In the fourth line, we introduce  $A(\underline{z}) = \prod_{n=0}^N A(z_n, z_{n-1})$ . The equation now takes the form of the partition of a classical Ising model with complex energies. Here,  $\underline{z}$  can be interpreted as a classical spin configuration,  $A(\underline{z})$  as the degeneracy number and  $i\frac{\pi}{4}\Phi(z_n, z_{n-1})$  as a complex energy associated with spin-spin interaction.

Further simplifications are possible by noticing that, the diagonal gates in the circuits allow the reduction of the number of classical spins. Specifically, if a  $T$  gate is applied to  $|z_{n-1}\rangle$ , it follows that  $z_n = z_{n-1}$ . Hence, the variables  $z_{n-1}$  and  $z_n$  can be represented by a single classical spin state. The two variables  $z_{n-1}, z_n$  become independent only when a non-diagonal gate is applied. Therefore, we can group all variables  $\{z_n\}$  between two non-diagonal gates as one classical spin. This procedure leads to the directives presented as the STEP I of the procedure in the previous section. Formally, for  $N_{\text{spin}} + 1$  non-diagonal gates in the circuit (including the first Hadamard gate)  $\underline{z}$  can be characterized by a classical spin configuration  $\underline{s} = (s_{-1}, s_0, \dots, s_k, \dots, s_{N_{\text{spin}}})$  where  $s_k = 1 - 2z_k \in \{\pm 1\}$  is a spin representing the basis variable immediately after the  $k^{\text{th}}$  non-diagonal gate, i.e.

$$p(z) = \left| \sum_{\underline{s} \in \{\pm 1\}^{N_{\text{spin}}+1}} A(\underline{s}) \exp \left[ \frac{i\pi}{4} \sum_{k=0}^{N_{\text{spin}}} \Phi(s_k, s_{k-1}) \right] \right|^2 \tag{B3}$$

$$= |Z_{\text{Ising}}|^2. \tag{B4}$$

Lastly, we need to specify  $A(\underline{s})$  and  $\Phi(s_k, s_{k-1})$  in term of the local fields  $h_{k-1}, h_k$ , the interaction  $J_{k-1,k}$ , and spin configurations  $s_{k-1}, s_k$ . This is done by first considering the gates in their matrix form, i.

$$\sqrt{X} = \frac{1}{\sqrt{2}} \begin{pmatrix} e^{\frac{i\pi}{2}} & 1 \\ 1 & e^{\frac{i\pi}{2}} \end{pmatrix} = \frac{1}{\sqrt{2}} \left[ e^{\frac{i\pi}{4}(1+s_k s_{k-1})} \right]_{s_k, s_{k-1}}, \tag{B5}$$

$$\sqrt{Y} = \frac{1}{\sqrt{2}} \begin{pmatrix} 1 & -1 \\ 1 & 1 \end{pmatrix} = \frac{1}{\sqrt{2}} \left[ e^{\frac{i\pi}{4}(1-s_{k-1})(1+s_k)} \right]_{s_k, s_{k-1}}, \tag{B6}$$

$$\sqrt{Y}^T = \frac{1}{\sqrt{2}} \begin{pmatrix} 1 & 1 \\ -1 & 1 \end{pmatrix} = \frac{1}{\sqrt{2}} \left[ e^{\frac{i\pi}{4}(1+s_{k-1})(1-s_k)} \right]_{s_k, s_{k-1}}, \tag{B7}$$

$$H = \frac{1}{\sqrt{2}} \begin{pmatrix} 1 & 1 \\ 1 & -1 \end{pmatrix} = \frac{1}{\sqrt{2}} \left[ e^{\frac{i\pi}{4}(1-s_{k-1})(1-s_k)} \right]_{s_k, s_{k-1}}, \tag{B8}$$

$$T = \begin{pmatrix} 1 & 0 \\ 0 & e^{\frac{i\pi}{4}} \end{pmatrix} = \text{Diag} \left[ e^{\frac{i\pi}{4}(\frac{1-s_k}{2})} \right]_{s_k} \tag{B9}$$

Notice that all non-diagonal gates contribute to the same amplitude  $A(s_k, s_{k-1}) = 1/\sqrt{2}$ , leading to  $A(\underline{s}) = 2^{-(N_{\text{spin}}+1)/2}$ . Hence, we can extract the contribution of each gate to  $\Phi(s_k, s_{k-1})$  as

$$\Phi_{\sqrt{X}}(s_k, s_{k-1}) = 1 + s_{k-1}s_k, \tag{B10}$$

$$\Phi_{\sqrt{Y}}(s_k, s_{k-1}) = (1 - s_{k-1})(1 + s_k) \tag{B11}$$

$$= 1 - s_{k-1} + s_k - s_{k-1}s_k, \tag{B12}$$

$$\Phi_{\sqrt{Y}^T}(s_k, s_{k-1}) = (1 + s_{k-1})(1 - s_k) \tag{B13}$$

$$= 1 + s_{k-1} - s_k - s_{k-1}s_k, \tag{B14}$$

$$\Phi_T(s_k) = \frac{1 - s_k}{2}. \tag{B15}$$

The under-script indicates which gate is contributing to the phase. The corresponding  $h_i, h_j$  and  $J_{ij}$  are depicted in the lookup table in figure 3(f), where  $i = k - 1$  and  $j = k$ . The global phase that does not depend on  $\underline{s}$  is ignored as it does not contribute to  $p(z)$ .

### B.2.2. Two-qubit example

Now we consider a two-qubit random circuits to demonstrate the action of the CZ gates. We introduce a new index  $l \in \{1, 2\}$  to label each qubit, which is placed on a given horizontal line (row). Since the CZ gate is diagonal, its presence does not alter the number of spins in each row. However, the gate introduces interaction between spins in different rows. This can be seen from its explicit form, i.e.

$$CZ = \begin{pmatrix} 1 & 0 & 0 & 0 \\ 0 & 1 & 0 & 0 \\ 0 & 0 & 1 & 0 \\ 0 & 0 & 0 & -1 \end{pmatrix} = \text{Diag} \left[ e^{\frac{i\pi}{4}(1-s_{1,k})(1-s_{2,k'})} \right]_{s_{1,k}, s_{2,k'}}, \tag{B16}$$

where  $s_{1,k}$  ( $s_{2,k'}$ ) is the state of the  $k^{\text{th}}$  ( $k'^{\text{th}}$ ) spin at the first (second) row. It follows that

$$\Phi_{s_{1,k}, s_{2,k'}}^{CZ} = (1 - s_{1,k})(1 - s_{2,k'}) \tag{B17}$$

$$= 1 - s_{1,k} - s_{2,k'} + s_{1,k}s_{2,k'}. \tag{B18}$$

The corresponding  $h_i$ ,  $h_j$ , and  $J_{ij}$  are depicted in figure 3(f) where  $i = (1, k)$  and  $j = (2, k')$ . We have now derived all necessary ingredients to map a random quantum circuit to a classical Ising model.

### B.2.3. Full COE dynamics

Since the COE dynamics can be expressed in terms of a quasi-random quantum circuit, we can straightforwardly apply the above procedure to find the corresponding Ising model. The complexity here solely arises from the number of indices required to specify the positions of all the gates in the circuit. To deal with this, we introduce the following indices

- an index  $l \in \{1, \dots, L\}$  to indicate which qubit / row.
- an index  $m \in \{1, \dots, M\}$  to indicate which period.
- an index  $\mu \in \{A, B\}$  to indicate which part of the period.  $A$  and  $B$  refer to the  $\hat{U}_{\text{CUE}}$  part and the  $\hat{U}_{\text{CUE}}^T$  part, respectively
- an index  $k \in \{0, 1, \dots, N_{\text{spin}}(l)\}$  to indicate the spin position for a given  $m$  and  $\mu$ . Here,  $N_{\text{spin}}(l)$  is the total number of spins at the  $l^{\text{th}}$  row. Note that due to the symmetric structure of  $\hat{U}_{\text{CUE}}$  and  $\hat{U}_{\text{CUE}}^T$ , we run the index  $k$  backward for the transpose part, i.e.  $k=0$  refers to the last layer.
- an index  $\nu_{l,k}$  so that  $\nu_{l,k} = 1$  if the  $k^{\text{th}}$  non-diagonal gate acting on the qubit  $l$  is  $\sqrt{X}$  otherwise  $\nu_{l,k} = 0$ .

With these indices, the partition function of the circuit, as shown in figure 3(a), can be written as

$$\langle \mathbf{z} | \psi \rangle = 2^{-\frac{G}{2}} \sum_{\mathbf{s} \in \mathcal{S}} \exp \left[ \frac{i\pi}{4} E(\mathbf{s}) \right], \quad (\text{B19})$$

with

$$\begin{aligned} E(\mathbf{s}) = E(\mathbf{z}) &+ \sum_{m=1}^M \sum_{\mu=A}^B \sum_{l=1}^L \sum_{k=0}^{N_{\text{spin}}(l)} h_{lk} s_{l,k}^{\mu,m} \\ &+ \sum_{m=1}^M \sum_{\mu=A}^B \sum_{l=1}^L \sum_{k=1}^{N_{\text{spin}}(l)} (2\nu_{l,k} - 1) s_{l,k-1}^{\mu,m} s_{l,k}^{\mu,m} \\ &+ \sum_{m=1}^M \sum_{\mu=A}^B \sum_{l=1}^L \sum_{l'=1}^{l-1} \sum_{k=1}^{N_{\text{spin}}(l)} \sum_{k'=1}^{N_{\text{spin}}(l')} \zeta_{(l,k)}^{(l',k')} s_{l,k}^{\mu,m} s_{l',k'}^{\mu,m}, \end{aligned} \quad (\text{B20})$$

and

$$h_{lk} = \nu_{l,k+1} - \nu_{l,k} - \frac{1}{2} N_T(l, k) - N_{CZ}(l, k), \quad (\text{B21})$$

$$E(\mathbf{z}) = -s_{0,l}^{B,M} - s_{z_l} + s_{0,l}^{B,M} s_{z_l}. \quad (\text{B22})$$

Here  $G$  is the total number of non-diagonal gates in the circuit.  $\zeta_{(l,k)}^{(l',k')}$  represents the total number of CZ gates which introduces the interaction between spins  $s_{l,k}^{\mu,m}$  and  $s_{l',k'}^{\mu,m}$ .  $N_{CZ}(l, k)$  ( $N_T(l, k)$ ) is the total number of CZ ( $T$ ) gates which introduces local fields on the spin  $s_{l,k}^{\mu,m}$ .  $E(\mathbf{z})$  is the contribution from the last Hadamard layer which depends on the readout bit-string  $\mathbf{z}$ .  $\{s_{z_l}\}$  are the spins corresponding to  $\mathbf{z}$  and their configuration is fixed. In addition, there are also two extra boundary conditions (i) between part  $A$  and  $B$  and (ii) between the two adjacent periods  $m$  and  $m+1$ , i.e.  $s_{l, N_{\text{spin}}(l)}^{A,m} = s_{l, N_{\text{spin}}(l)}^{B,m}$  and  $s_{l,0}^{A,m+1} = s_{l,0}^{B,m}$ .

## Appendix C. Derivation of Porter-Thomas distribution from COE dynamics.

In this section, we provide additional mathematical details involved in the proof of theorem 2. More precisely, we show that the distribution of the output probability of COE dynamics,  $\text{Pr}(p)$ , follows the Porter-Thomas distribution  $\text{Pr}_{\text{PT}}(p) = N e^{-Np}$ . First, let us consider the output probability  $\tilde{p}_M(\mathbf{z}) = |\langle \mathbf{z} | \psi_M \rangle|^2$  with



$$\begin{aligned}
 \langle \mathbf{z} | \psi_M \rangle &= \langle \mathbf{z} | U_{\text{COE}}^M | 0 \rangle \\
 &= \langle \mathbf{z} | \left[ \sum_{\epsilon=0}^{N-1} e^{iME_\epsilon T} | E_\epsilon \rangle \langle E_\epsilon | \right] | 0 \rangle \\
 &= \sum_{\epsilon=0}^{N-1} d_\epsilon(\mathbf{z}) e^{i\phi_{M,\epsilon}} \\
 &= \left[ \sum_{\epsilon=0}^{N-1} d_\epsilon(\mathbf{z}) \cos \phi_{M,\epsilon} \right] + i \left[ \sum_{\epsilon=0}^{N-1} d_\epsilon(\mathbf{z}) \sin \phi_{M,\epsilon} \right] \\
 &= a_{\mathbf{z}} + ib_{\mathbf{z}},
 \end{aligned} \tag{C1}$$

where  $N$  is the dimension of the Hilbert space,  $d_\epsilon(\mathbf{z}) = \langle \mathbf{z} | E_\epsilon \rangle \langle E_\epsilon | 0 \rangle$ ,  $\phi_{m,\epsilon} = ME_\epsilon T \text{ mod } 2\pi$ ,  $a_{\mathbf{z}} = \text{Re}[\langle \mathbf{z} | \psi_M \rangle]$  and  $b_{\mathbf{z}} = \text{Im}[\langle \mathbf{z} | \psi_M \rangle]$ .

**Lemma 1.** *The distribution of  $d_\epsilon(\mathbf{z})$  over  $\forall \epsilon \in \{0, \dots, N-1\}$  or  $\forall \mathbf{z} \in \{0, 1\}^L$  is the Bessel function of the second kind.*

**Lemma 2.** *The distribution of  $a_{\mathbf{z}}$  and  $b_{\mathbf{z}}$  over  $\forall \mathbf{z} \in \{0, 1\}^L$  is the normal distribution with zero mean and variance equal to  $1/2N$ .*

To prove lemma 1, we first write  $d_\epsilon(\mathbf{z}) = c_{\mathbf{z},\epsilon} c_{0,\epsilon}$ , where  $c_{\mathbf{z},\epsilon} = \langle \mathbf{z} | E_\epsilon \rangle$  and  $c_{0,\epsilon} = \langle 0 | E_\epsilon \rangle$ . For the COE dynamics, the coefficients  $c_{\mathbf{z},\epsilon}$  and  $c_{0,\epsilon}$  are real numbers whose distribution is [45]

$$\text{Pr}(c) = \sqrt{\frac{2N}{\pi}} \exp\left[-\frac{Nc^2}{2}\right]. \tag{C2}$$

As discussed in the main text, the phase  $\phi_{M,\epsilon}$  becomes random as  $M \gg 2\pi/E_\epsilon T$ . The random sign ( $\pm 1$ ) from  $c_{\mathbf{z},\epsilon}$  can therefore be absorbed into the phase without changing its statistics. The distribution of  $d_\epsilon(\mathbf{z})$  can be obtained using the product distribution formula

$$\begin{aligned}
 \text{Pr}(d) &= \int_0^\infty \text{Pr}(c) \text{Pr}\left(\frac{d}{c}\right) \cdot \frac{1}{c} \cdot dc \\
 &= \frac{2N}{\pi} \int_0^\infty \exp\left(-\frac{Nc^2}{2}\right) \exp\left(-\frac{Nd^2}{2c^2}\right) dc \\
 &= \frac{2N}{\pi} K_0(Nd),
 \end{aligned} \tag{C3}$$

where  $K_0$  is the modified Bessel function of the second kind.

To prove lemma 2, we first note that the distribution of  $\cos \phi_{m,\epsilon}$  and  $\sin \phi_{m,\epsilon}$  with  $\phi_{M,\epsilon}$  being uniformly distributed in the range  $[0, 2\pi)$  are

$$\text{Pr}(\cos \phi) = \frac{1}{\pi \sqrt{1 - \cos^2 \phi}}, \tag{C4}$$

$$\text{Pr}(\sin \phi) = \frac{1}{\pi \sqrt{1 - \sin^2 \phi}}. \tag{C5}$$

We then calculate the distribution of  $\kappa_\epsilon \equiv d_\epsilon(\mathbf{z}) \cos \phi_{M,\epsilon}$  using the product distribution formula, i.e.

$$\text{Pr}(\kappa) = \int_{-1}^1 \frac{1}{\pi \sqrt{1 - \cos^2 \phi}} \cdot \frac{2N}{\pi} K_0\left(\frac{N\kappa}{d}\right) \cdot \frac{1}{\cos \phi} d \cos \phi = \frac{N}{\pi^2} K_0^2\left(\frac{N|\kappa|}{2}\right). \tag{C6}$$

The mean and the variance of  $\kappa_\epsilon$  can be calculated as

$$\langle \kappa \rangle = \int_{-\infty}^{\infty} d \cos \phi \cdot \frac{N}{\pi^2} \cdot K_0^2 \left( \frac{N|\kappa|}{2} \right) \cdot d\kappa = 0 \quad (\text{C7})$$

$$\text{Var}(\kappa) = \int_{-\infty}^{\infty} (d \cos \phi)^2 \cdot \frac{N}{\pi^2} \cdot K_0^2 \left( \frac{N|\kappa|}{2} \right) \cdot d\kappa = \frac{1}{2N^2}. \quad (\text{C8})$$

Since  $a_z$  is a sum of independent and identically distributed random variables, i.e.  $a_z = \sum_{\epsilon=1}^{N-1} \kappa_\epsilon$ , we can apply the central limit theorem for large  $N$ . Hence, the distribution of  $a_z$  is normal with the mean zero and variance  $\text{Var}(a) = N \cdot \text{Var}(\kappa) = 1/2N$ . The same applies for the distribution of  $b_z$ .

Theorem 2 can be proven using the fact that the sum of the square of Gaussian variables follows the  $\chi$ -squared distribution with second degree of freedom  $\text{Pr}_{\chi^2, k=2}(p) \sim \exp\{-p/2\sigma^2\}$  [47]. By specifying the variance obtained in Lemma 2 and normalization, the distribution of  $p_M(\mathbf{z}) = a_z^2 + b_z^2$  over  $\forall \mathbf{z} \in \{0, 1\}^L$  is the Porter-Thomas distribution. Since the Porter Thomas distribution anti-concentrates i.e.  $\text{Pr}_{\text{PT}}(p > \frac{1}{N}) = \int_{Np=1}^{\infty} d(Np)e^{-Np} = 1/e$ , we complete the proof of the theorem 2.

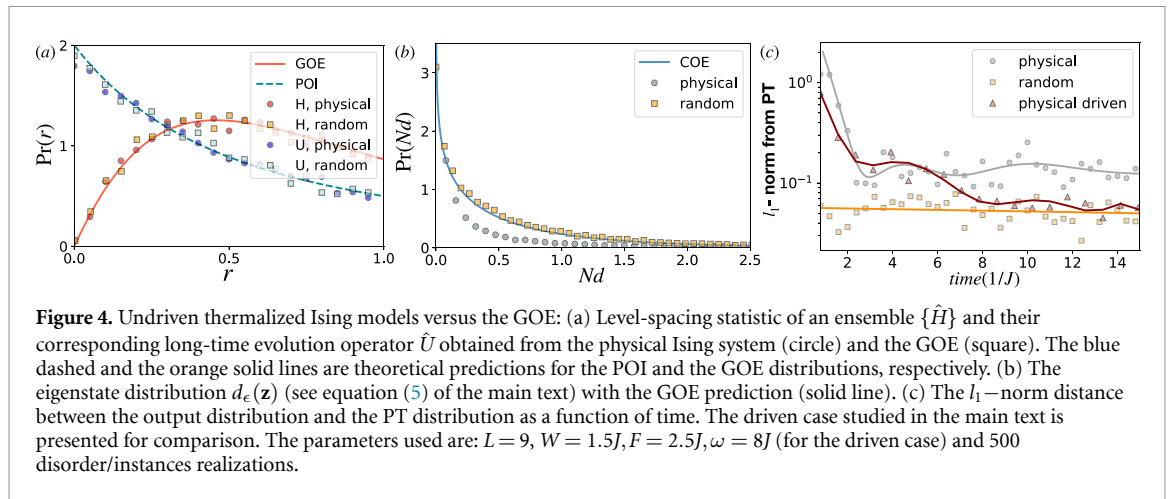
## Appendix D. Undriven thermalized many-body systems

In this section, we analyze the long-time unitary evolution for undriven systems in the thermalized phase. The results presented here highlight the key role played by the drive in generating the randomness required for the above quantum supremacy proof. In particular, we show that for typical undriven physical systems with local constraints (e.g. finite-range interactions) and conserved energy, the output distribution never coincides with the PT distribution.

We emphasize that this is a consequence of the inability of random matrix theory to accurately describe the full spectral range of undriven thermalized many-body systems. Indeed, it has been shown that for undriven many-body systems which thermalizes (to a finite temperature), the statistics of the Hamiltonian resembles the statistics of the Gaussian orthogonal ensemble (GOE) [28]. However, it is implicit that an accurate match only applies over a small energy window (usually far from the edges of the spectrum). If one zooms in this small energy window, the Hamiltonian looks random, but if one consider the full spectrum, the local structure of the Hamiltonian appears and the random matrix theory fails at capturing it.

To see this, we numerically simulate the undriven Ising Hamiltonian,  $\hat{H}_0 = \sum_{l=0}^{L-1} \mu_l \hat{Z}_l + J \sum_{l=0}^{L-2} \hat{Z}_l \hat{Z}_{l+1} + \frac{F}{2} \sum_{l=0}^{L-1} \hat{X}_l$ , where  $\mu_l \in \{0, W\}$  is a local disorder,  $W$  is the disorder strength,  $F$  is the static global magnetic field along  $x$  and  $J$  is the interaction strength. This Hamiltonian is in fact the average Hamiltonian of the driven Ising Hamiltonian used in the main text. In comparison, we also simulate the quantum evolution under an ensemble  $\{\hat{H}_{\text{COE}}\}$  of synthetic Hamiltonians that are uniformly drawn from the GOE (i.e. without any local constraints).

Figure 4(a) shows the level-spacing statistics of  $\{\hat{H}_0\}$  (obtained over 500 disorder realizations),  $\{\hat{H}_{\text{COE}}\}$  (obtained over 500 random instances) and their corresponding long-time unitary operators  $\hat{U} = \lim_{t \rightarrow \infty} e^{-i\hat{H}t}$ . We see that the level statistic of the physical Hamiltonian (and its long-time evolution) is indistinguishable from the GOE. However, the discrepancy between the physical and synthetic (GOE) realizations becomes apparent when looking at the eigenstate statistics as shown in figure 4(b). While the distribution of  $d_\epsilon(\mathbf{z})$  (see equation (5) of the main text) from the GOE is in a good agreement with the Bessel function of the second kind, the physical system fails to meet the theoretical prediction. This is in contrast to the driven case as presented in the main text. More importantly in the context of this work, a key difference between the physical Hamiltonian and the random matrix theory prediction can be seen by comparing the distribution of the output states after some time evolution. In figure 4(c), we show that the Porter-Thomas distribution is never achieved with the physical systems while it is for the synthetic realizations as well as for the driven case studied in the main text. These results underline the gap between physical Hamiltonians and true random matrices and more importantly, they highlights the important role of the drive in bridging that gap.



## ORCID iD

Supanut Thanasilp  <https://orcid.org/0000-0002-8252-4056>

## References

- [1] Preskill J 2018 Quantum Computing in the NISQ era and beyond *Quantum* **2** 79
- [2] Harrow A W and Montanaro A 2017 Quantum computational supremacy *Nature* **549** 203–9
- [3] Aaronson S and Arkhipov A 2011 The computational complexity of linear optics *Proc. 43rd Annual ACM Symp. on Theory of Computing (STOC 2011)* pp 333–42
- [4] Aaronson S 2011 A linear-optical proof that the permanent is #P-hard *Proc. R. Soc. A* **467** 3393
- [5] Lund A P, Bremner M J and Ralph T C 2017 Quantum sampling problems, bosonsampling and quantum supremacy *npj Quantum Inf.* **3** 15
- [6] Bremner M J, Jozsa R and Shepherd D J 2011 Classical simulation of commuting quantum computations implies collapse of the polynomial hierarchy *Proc. R. Soc. A* **467** 459–72
- [7] Boixo S, Isakov S V, Smelyanskiy V N, Babbush R, Ding N, Jiang Z, Bremner M J, Martinis J M and Neven H 2018 Characterizing quantum supremacy in near-term devices *Nat. Phys.* **14** 595–600
- [8] Bouland A, Fefferman B, Nirkhe C and Vazirani U 2019 On the complexity and verification of quantum random circuit sampling *Nat. Phys.* **15** 159–63
- [9] Spring J B et al 2013 Boson sampling on a photonic chip *Science* **339** 798–801
- [10] Broome M A, Fedrizzi A, Rahimi-Keshari S, Dove J, Aaronson S, Ralph T C and White A G 2013 Photonic boson sampling in a tunable circuit *Science* **339** 794–8
- [11] Tillmann M, Dakić B, Heilmann R, Nolte S, Szameit A and Walther P 2013 Experimental boson sampling *Nat. Photon.* **7** 540
- [12] Crespi A, Osellame R, Ramponi R, Brod D J, Galvão E F, Spagnolo N, Vitelli C, Maiorino E, Mataloni P and Sciarrino F 2013 Integrated multimode interferometers with arbitrary designs for photonic boson sampling *Nat. Photon.* **7** 545–9
- [13] Wang H et al 2019 Boson sampling with 20 input photons and a 60-mode interferometer in a  $10^{14}$ -dimensional hilbert space *Phys. Rev. Lett.* **123** 250503
- [14] Zhong H-S et al 2020 Quantum computational advantage using photons *Science* **370** 1460–3
- [15] Zhong H-S et al 2021 Phase-programmable gaussian boson sampling using stimulated squeezed light *Phys. Rev. Lett.* **127** 180502
- [16] Madsen L S et al 2022 Quantum computational advantage with a programmable photonic processor *Nature* **606** 75–81
- [17] Neill C et al 2018 A blueprint for demonstrating quantum supremacy with superconducting qubits *Science* **360** 195–9
- [18] Arute F et al 2019 Quantum supremacy using a programmable superconducting processor *Nature* **574** 505–10
- [19] Wu Y et al 2021 Strong quantum computational advantage using a superconducting quantum processor *Phys. Rev. Lett.* **127** 180501
- [20] Cirac J I and Zoller P 2012 Goals and opportunities in quantum simulation *Nat. Phys.* **8** 264–6
- [21] Hauke P, Cucchiatti F M, Tagliacozzo L, Deutsch I and Lewenstein M 2012 Can one trust quantum simulators? *Rep. Prog. Phys.* **75** 082401
- [22] Johnson T H, Clark S R and Jaksch D 2014 What is a quantum simulator? *EPJ Quantum Technol.* **1** 10
- [23] Georgescu I M, Ashhab S and Nori F 2014 Quantum simulation *Rev. Mod. Phys.* **86** 153–85
- [24] Choi J-Y, Hild S, Zeiher J, Schauß P, Rubio-Abadal A, Yefsah T, Khemani V, Huse D A, Bloch I and Gross C 2016 Exploring the many-body localization transition in two dimensions *Science* **352** 1547–52
- [25] Bermejo-Vega J, Hangleiter D, Schwarz M, Raussendorf R and Eisert J 2018 Architectures for quantum simulation showing a quantum speedup *Phys. Rev. X* **8** 021010
- [26] Gao X, Wang S-T and Duan L-M 2017 Quantum supremacy for simulating a translation-invariant ising spin model *Phys. Rev. Lett.* **118** 040502
- [27] Novo L, Bermejo-Vega J and García-Patrón Rul 2019 Quantum advantage from energy measurements of many-body quantum systems (arXiv:1912.06608)
- [28] D'Alessio L, Kafri Y, Polkovnikov A and Rigol M 2016 From quantum chaos and eigenstate thermalization to statistical mechanics and thermodynamics *Adv. Phys.* **65** 239–362
- [29] D'Alessio L and Rigol M 2014 Long-time behavior of isolated periodically driven interacting lattice systems *Phys. Rev. X* **4** 041048
- [30] Bordia P, Lüschen H, Schneider U, Knap M and Bloch I 2017 Periodically driving a many-body localized quantum system *Nat. Phys.* **13** 460–4

- [31] Singh K *et al* 2019 Quantifying and controlling prethermal nonergodicity in interacting floquet matter *Phys. Rev. X* **9** 041021
- [32] Wintersperger K, Bukov M, Näger J, Lellouch S, Demler E, Schneider U, Bloch I, Goldman N and Aidelsburger M 2020 Parametric instabilities of interacting bosons in periodically driven 1D optical lattices *Phys. Rev. X* **10** 011030
- [33] Monroe C, Campbell W C, Duan L, Gong Z-X, Gorshkov A V, Hess P, Islam R, Kim K, Linke N, Pagano G, Richerme P, Senko C and Yao N 2019 Programmable quantum simulations of spin systems with trapped ions (arXiv:1912.07845)
- [34] Otterbach J S *et al* Unsupervised Machine Learning on a Hybrid Quantum Computer
- [35] Rubio-Abadal A, Ippoliti M, Hollerith S, Wei D, Rui J, Sondhi S L, Khemani V, Gross C and Bloch I 2020 Floquet prethermalization in a Bose-Hubbard system (arXiv:2001.08226)
- [36] Eckardt Ae 2017 Colloquium: atomic quantum gases in periodically driven optical lattices *Rev. Mod. Phys.* **89** 011004
- [37] Zheng Y-G, Zhang W-Y, Shen Y-C, Luo A, Liu Y, Ming-Gen H, Zhang H-R, Lin W, Wang H-Y, Zhu Z-H, Chen M-C, Chao-Yang L, Thanasilp S, Angelakis D G, Yuan Z-S and Pan J-W 2022 Efficiently extracting multi-point correlations of a floquet thermalized system (arXiv:2210.08556)
- [38] Eisert J, Friesdorf M and Gogolin C 2015 Quantum many-body systems out of equilibrium *Nat. Phys.* **11** 124–30
- [39] Hangleiter D and Eisert J 2022 Computational advantage of quantum random sampling (arXiv:2206.04079)
- [40] Eisert J, Hangleiter D, Walk N, Roth I, Markham D, Parekh R, Chabaud U and Kashefi E 2020 Quantum certification and benchmarking *Nat. Rev. Phys.* **2** 382–90
- [41] Hangleiter D, Bermejo-Vega J, Schwarz M and Eisert J 2018 Anticoncentration theorems for schemes showing a quantum speedup *Quantum* **2** 65
- [42] Stockmeyer L 1985 On approximation algorithms for #P *SIAM J. Comput.* **14** 849–61
- [43] Ann Goldberg L A and Guo H 2017 The complexity of approximating complex-valued ising and tutte partition functions *Comput. Complex.* **26** 765–833
- [44] Bremner M J, Montanaro A and Shepherd D J 2016 Average-Case complexity versus approximate simulation of commuting quantum computations *Phys. Rev. Lett.* **117** 080501 (Publisher: American Physical Society)
- [45] Haake F 2010 *Quantum Signatures of Chaos* (New York: Springer)
- [46] Thanasilp S, Tangpanitanon J, Lemonde M-A, Dangniam N and Angelakis D G 2021 Quantum supremacy and quantum phase transitions *Phys. Rev. B* **103** 165132
- [47] Marvin K S 2002 *Probability Distributions Involving Gaussian Random Variables* (Boston, MA: Springer)
- [48] Kim H, Ikeda T N and Huse D A 2014 Testing whether all eigenstates obey the eigenstate thermalization hypothesis *Phys. Rev. E* **90** 052105
- [49] Lazarides A, Das A and Moessner R 2014 Equilibrium states of generic quantum systems subject to periodic driving *Phys. Rev. E* **90** 012110
- [50] Mori T, Kuwahara T and Saito K 2016 Rigorous bound on energy absorption and generic relaxation in periodically driven quantum systems *Phys. Rev. Lett.* **116** 120401
- [51] Abanin D A, Altman E, Bloch I and Serbyn M 2019 Colloquium: many-body localization, thermalization and entanglement *Rev. Mod. Phys.* **91** 021001
- [52] Mori T, Ikeda T N, Kaminishi E and Ueda M 2018 Thermalization and prethermalization in isolated quantum systems: a theoretical overview *J. Phys. B: At. Mol. Opt. Phys.* **51** 112001
- [53] Tangpanitanon J, Thanasilp S, Dangniam N, Lemonde M-A and Angelakis D G 2020 Expressibility and trainability of parametrized analog quantum systems for machine learning applications *Phys. Rev. Res.* **2** 043364
- [54]  $f(n) = o(g(n))$  means that  $f(n)/g(n) \rightarrow 0$  when  $n \rightarrow \infty$
- [55] Roberts D A and Yoshida B 2017 Chaos and complexity by design *J. High Energy Phys.* **2017** 121
- [56] Harrow A W and Low R A 2009 Random quantum circuits are approximate 2-designs *Commun. Math. Phys.* **291** 257–302
- [57] Nicholas R J 2018 Chaos and randomness in strongly-interacting quantum systems *Dissertation (PhD)* California Institute of Technology